AIAA JOURNAL
Vol. 45, No. 10, October 2007

Suppressing Aeroelastic Instability Using Broadband Passive Targeted Energy Transfers, Part 2: Experiments

Young S. Lee*
University of Illinois at Urbana–Champaign, Urbana, Illinois 61801
Gaëtan Kerschen†
University of Liège, 4000 Liège, Belgium
D. Michael McFarland‡
University of Illinois at Urbana–Champaign, Urbana, Illinois 61801
W. Joel Hill,§ Chetan Nichkawde,¶ and Thomas W. Strganac**
Texas A&M University, College Station, Texas 77843
Lawrence A. Bergman††
University of Illinois at Urbana–Champaign, Urbana, Illinois 61801
and
Alexander F. Vakakis‡‡
National Technical University of Athens, GR-157 10 Athens, Greece

DOI: 10.2514/1.28300

This paper presents experimental results corroborating the analysis developed in the companion paper, Part 1 (Lee, Y., Vakakis, A., Bergman, L., McFarland, M., and Kerschen G., "Suppression Aeroelastic Instability Using Broadband Passive Targeted Energy Transfers, Part 1: Theory," *AIAA Journal*, Vol. 45, No. 3, 2007, pp. 693–711), and demonstrates that a nonlinear energy sink can improve the stability of an aeroelastic system. The nonlinear energy sink was, in this case, attached to the heave (plunge) degree of freedom of a rigid airfoil which was supported in a low-speed wind tunnel by nonlinear springs separately adjustable in heave and pitch. This airfoil was found to exhibit a limit cycle oscillation at flow speeds above the critical ("flutter") speed of 9.5 m/s, easily triggered by an initial heave displacement. After attachment of a single degree of freedom, essentially nonlinear energy sink to the wing, the combined system exhibited improved dynamic response as measured by the reduction or elimination of limit cycle oscillation at flow speeds significantly greater than the wing's critical speed. The design, application, and performance of the nonlinear energy sink are described herein, and the results obtained are compared to analytical predictions. The physics of the interaction of the sink with the wing is examined in detail.

I. Introduction

WHILE uncommon in some types of aircraft operations, the phenomenon of aeroelastic instability is often limiting in others. Military aircraft flying at transonic speeds, or with varying configurations of external stores, are especially prone to instabilities such as limit cycle oscillation (LCO). Denegri [1] and Bunton and Denegri [2] observed limit cycle oscillations in flight tests of the F-16 and F/A-18 when certain wing-mounted stores were present. Croft [3] discussed limit cycle oscillations in the elevators of several Airbus passenger airplanes. The development of divergent flutter, leading to immediate structural failure, is rare, but sustained LCO can cause structural damage, including fatigue. In addition, the need to avoid flight conditions (speeds, attitudes, and aircraft configurations) conducive to instability leads to onerous restrictions on operations and increased pilot workload. The establishment of safe flight envelopes often requires extensive and costly flight-test programs, which must be repeated for each change in aircraft configuration (e.g., the introduction of a new type of external store).

Many authors have studied the causes of limit cycle oscillations. The common factor in all aircraft systems exhibiting limit cycle behavior is aeroelastic nonlinearities. These nonlinearities can exist in the flowfield, the structure, or both. Dowell et al. [4] provides an excellent summary of recent studies done in the fields of aerodynamics and structural dynamics to understand nonlinear aeroelasticity. Cunningham [5] and Hartwich et al. [6] examined nonlinear aerodynamics and the contributions these nonlinearities make to producing LCOs. Chen et al. [7] described the role of nonlinear structural damping in the development of LCOs, and Gilliatt et al. [8] and Thompson and Strganac [9] examined the influence of internal resonance on LCO behavior.

Stiffness nonlinearity was examined by Tang and Dowell [10], who described LCO as the interaction of the nonlinear structure with nonlinear aerodynamics and provided experimental and theoretical results. Many analytical studies of nonlinear stiffness were

Received 10 October 2006; revision received 2 June 2007; accepted for publication 19 June 2007.

*Graduate Research Assistant, Department of Mechanical Science and Engineering, 1206 West Green Street; yslee4@uiuc.edu.

†Postdoctoral Researcher, Aerospace and Mechanical Engineering Department (LTAS), Chemin des Chevreuils (B52/3) 4000; g.kerschen@ulg.ac.be; currently Visiting Scholar, Department of Aerospace Engineering, University of Illinois at Urbana–Champaign, Urbana, IL 61801.

‡Research Associate Professor, Department of Aerospace Engineering, 104 South Wright Street; dmmcf@uiuc.edu. Senior Member AIAA.

§Graduate Research Assistant, Department of Aerospace Engineering; jhill@tamu.edu. Member AIAA.

¶Graduate Research Assistant, Department of Aerospace Engineering. Member AIAA.

**Professor, Department of Aerospace Engineering; strag@tamu.edu. Associate Fellow AIAA.

††Professor, Department of Aerospace Engineering, 104 South Wright Street; lbergman@uiuc.edu. Associate Fellow AIAA.

‡‡Professor, School of Applied Mathematical and Physical Sciences, P. O. Box 64042, GR-157 10, Zografos, Greece; vakakis@central.ntua.gr; currently Adjunct Professor, Department of Mechanical Science and Engineering and Department of Aerospace Engineering, University of Illinois at Urbana–Champaign, Urbana, IL 61801.

performed by O'Neil [11], O'Neil et al. [12], Sheta et al. [13], and Thompson and Strganac [9]. These were all experimentally validated using the nonlinear aeroelastic test apparatus (NATA) in a low-speed wind tunnel at Texas A&M University.

Many authors have also studied methods for controlling or suppressing limit cycle oscillations. Ko et al. [14] and Block and Strganac [15] developed several control laws using linear theory, partial feedback linearization, and adaptive control to stabilize an inherently unstable aeroelastic system with a single trailing-edge control surface. Platanitis and Strganac [16] used feedback linearization and model reference adaptive control to stabilize an aeroelastic system with leading- and trailing-edge control surfaces. These authors have shown that active control can be used to raise the threshold velocity above which LCOs occur. Although active control has been shown to be effective in suppressing LCOs, these methods require significant use of control resources. Active methods also require sensors capable of constantly providing accurate measurements for feedback into the controller.

That new fundamental insights into the conditions leading to LCO development and the underlying dynamical mechanisms continue to emerge is a reflection of the difficulty and complexity of the problem, but these developments also offer new opportunities to address the limitations posed by instabilities. It is one such advance that forms the basis for the work reported in this paper and its companion, Part 1 [17]. Specifically, knowledge of the sequence of energy transfers and resonance captures occurring during the onset of LCO of a rigid airfoil on nonlinear elastic supports, described by Lee et al. [18], can be exploited to suppress (reduce or eliminate) this LCO. This is achieved through the attachment of a passive, lightweight, single-degree-of-freedom (SDOF) module, a nonlinear energy sink (NES), coupled to one or both of the degrees of freedom of the wing through an essentially nonlinear spring. The dynamics of the combined system thus formed have been studied extensively, with the results reported in Part 1 [17]. In this second part, the experimental validation of that analysis is described.

A series of earlier papers [19–28] discusses targeted energy transfer (TET), or "energy pumping," from a directly excited primary structure to an NES. The NES is a simple, fully passive device that is able to dramatically modify the global dynamics of the system it is attached to despite being a local modification. We have demonstrated by analysis and simulation that the implementation of the NES on a Van der Pol oscillator, which is well known to exhibit limit cycle behavior, leads to complete suppression of the LCO over a wide range of the NES parameter space [29]. We have examined the well-known and long-used aeroelastic scenario of a cubically nonlinear rigid wing in a quasi-steady flowfield and shown, for the first time, that LCO formation is a consequence of a series of resonance captures and escapes, and that the heave mode is the unique trigger for the pitch mode LCO [18]. And we have implemented the NES on an aeroelastic system and have shown that, as in the Van der Pol system, suppression occurs over a broad range of NES parameters in three distinct mechanisms: alternate bursting and elimination, complete elimination, and attenuation. The last of these applications of the NES is reported in this paper.

The potentially unstable aeroelastic structure considered herein is a rigid airfoil in a low-speed wind tunnel. This wing was mounted on separately adjustable springs restraining its motion in heave (plunge) and pitch. This apparatus has been used by Strganac et al. in several experiments on passive and active aeroelastic control [14–16], in the course of which it has been very thoroughly characterized. In the absence of any corrective measures, this wing has a critical speed of approximately 9.5 m/s. When the flow speed in the wind tunnel exceeds this value, LCO can readily be induced by a small initial displacement of the heave degree of freedom. An NES was designed to be coupled to this airfoil's heave motion, with the goal of increasing the critical speed of the combined system above that of the wing alone. In this paper, we compare measured responses of the wing and of the wing-NES system to predictions from analysis and simulation in an effort to both quantify the performance improvement and verify our analysis of the underlying dynamics.

II. Experimental Apparatus and Procedures

The hardware used in the tests reported below is broadly divisible into the wind tunnel, the model wing, and its supporting structure; the nonlinear energy sink and its support; and the equipment used to measure the response of both substructures. These systems are described separately in the following sections.

A. Wind-Tunnel Model of 2-DOF Rigid Wing

The NATA at Texas A&M University was developed to experimentally test linear and nonlinear aeroelastic behavior. The device consists of a rigid NACA 0015 wing section capable of movement with 2 degrees of freedom, pitch, and heave, as shown schematically in Fig. 1. Stiffness nonlinearity can be introduced in either degree of freedom. The device is mounted in a 0.61×0.91 m low-speed wind tunnel capable of speeds up to 45 m/s. Each degree of freedom of the NATA wing is supported by its own set of springs. Heave motion, which mimics out-of-plane bending of the wing, is provided by mounting the wing on a carriage which can slide from side to side on shafts mounted under the wind tunnel. The motion of the carriage is restricted by springs stretching from the rigid frame of the wind tunnel to a rotating cam. The carriage is attached to the same cam such that its movement is resisted by the springs, as shown in

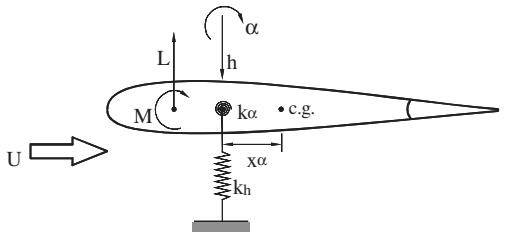

Fig. 1 A typical two-dimensional aeroelastic wing with 2 degrees of freedom, heave *h* and pitch α.

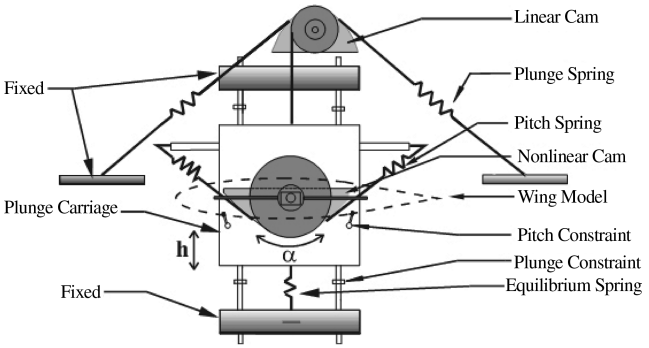

Fig. 2 The supporting structure of the nonlinear aeroelastic test apparatus (NATA).

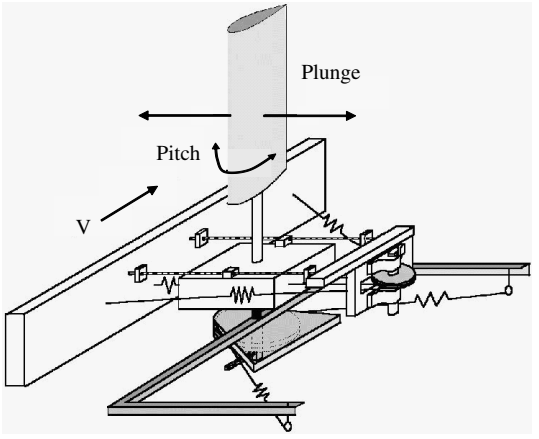

Fig. 3 Schematic of the NATA.

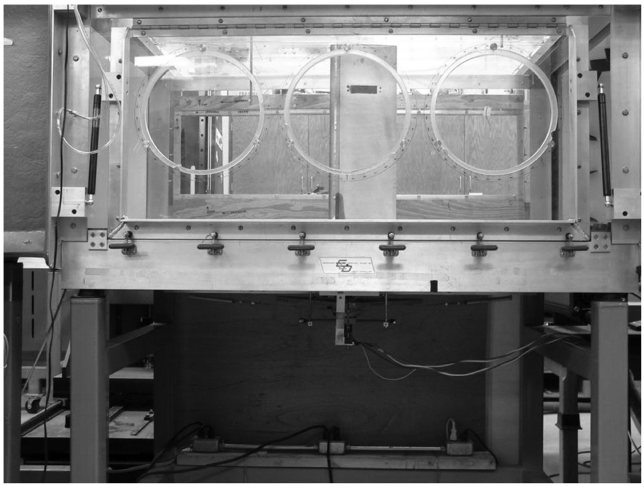

Fig. 4 Photo of the NATA. Air flow is left to right. The plunge carriage and pitch cam are visible beneath the tunnel.

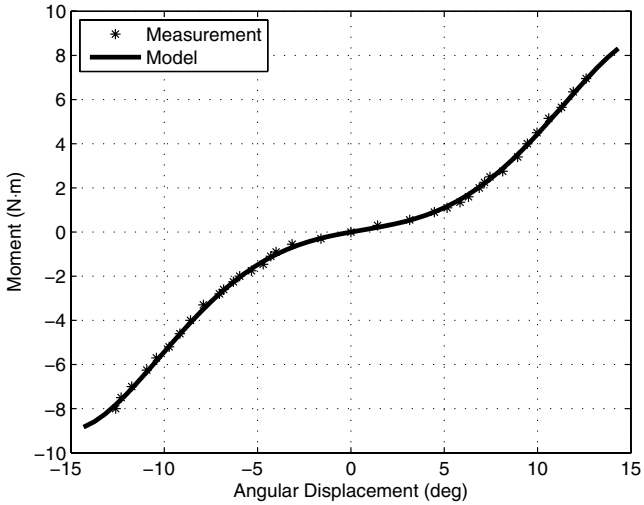

Fig. 5 Measured stiffness and fitted model of NATA pitch spring.

Figs. 2 and 3. The wing section stands vertically in the wind tunnel, spanning the entire tunnel from top to bottom, as shown in Fig. 4. The wing is attached to a shaft that exits through the tunnel floor and mounts via rotational bearings to the plunge carriage beneath the tunnel. These bearings allow the wing to pitch (rotate), simulating torsion of the wing. The pitch springs each have one end rigidly fixed to the plunge carriage. Their other ends wrap around a cam on the pitch shaft. A photograph of the NATA, depicting the wing section inside the wind tunnel and the plunge carriage and pitch cam below the tunnel, is shown in Fig. 4.

The shape of the cams in each degree of freedom determines whether the response will be linear or nonlinear. A circular cam gives a linear spring force while a nonlinear (e.g., parabolic) cam provides a hardening stiffness. Each degree of freedom can be made linear or nonlinear independent of the other. All tests described herein used a linear plunge cam and a nonlinear pitch cam.

The equation of motion of the NATA may be written

$$M\ddot{x} + C\dot{x} + Kx = F_c + F_a \tag{1}$$

where

$$x(t) = \{h(t) \;\; \alpha(t)\}^T \tag{2}$$

with h and α being the wing heave and pitch displacements, respectively, F_c embodies Coulomb friction forces, and

$$F_a = \{-L \;\; M\}^T \tag{3}$$

contains the aerodynamic force and moment on the wing. In Eq. (1), M is a mass matrix, C a damping matrix which includes a nonlinear kinematic term, and K a stiffness matrix. These matrices are expressed in terms of the physical parameters of the system, defined in Table 1, as

$$M = \begin{bmatrix} m_T & m_w r_{\text{cg}} \cos\alpha - m_c r_c \sin\alpha \\ m_w r_{\text{cg}} \cos\alpha - m_c r_c \sin\alpha & I_\alpha \end{bmatrix} \tag{4a}$$

$$C = \begin{bmatrix} C_h & -(m_w r_{\text{cg}} \sin\alpha + m_c r_c \cos\alpha)\dot{\alpha} \\ 0 & c_\alpha \end{bmatrix} \tag{4b}$$

and

$$K = \begin{bmatrix} k_h & 0 \\ 0 & k_\alpha(\alpha) \end{bmatrix} \tag{4c}$$

The stiffness in pitch is denoted $k_\alpha(\alpha)$ to signify that the nonlinear stiffness is a function of α, and is represented by

$$k_\alpha(\alpha) = 8.6031 - 27.67\alpha + 867.15\alpha^2 + 376.64\alpha^3 - 7294.6\alpha^4 \tag{5}$$

the result of a least-squares fit to measurements of angular displacement of the system and the restoring moment created by the nonlinear pitch cam. The stiffness model of Eq. (5) and the measured moment values are plotted versus angular displacement in Fig. 5.

Experiments using the NATA are conducted at very low speeds and at very low reduced frequency. The wing section spans the entire wind tunnel, so the flow can be considered two dimensional. For this tame flow environment, lift and drag can be modeled with quasi-steady aerodynamics. This type of aerodynamic model has provided very good agreement with NATA experimental results in the past. Friction has a significant effect on the dynamic behavior of the NATA system; both viscous damping and Coulomb friction appear in Eq. (1).

Table 1 NATA parameter values

Parameter	Symbol	Value	Units
Wing mass	m_w	1.645	kg
Pitch cam mass	m_c	0.714	kg
Total plunging mass	m_T	12.1	kg
Total pitching inertia	I_α	$0.04561 + m_w r_{\text{cg}}^2$	$\text{kg} \cdot \text{m}^2$
Wing mass offset	r_{cg}	$-b(a + 0.18)$	m
Wing section semichord	b	0.1064	m
Nondimensional elastic axis location	a	−0.4	——
Pitch cam mass offset	r_c	0.127	m
Viscous plunge damping coefficient	c_h	5.0747	kg/s
Viscous pitch damping coefficient	c_α	0.015	$\text{kg} \cdot \text{m}^2/\text{s}$
Plunge spring stiffness	k_h	2537.2	N/m
Pitch spring stiffness	k_α	Equation (5)	$\text{N} \cdot \text{m/rad}$
Wing section span	s	0.6	m

B. Addition of the Nonlinear Energy Sink

For the first proof-of-concept experiments with an NES in an aerodynamic application, the design goals were similar to what would be desired of flight hardware, tempered by the realities of the laboratory environment and the scale of the test program. It was desired to design a lightweight, passive, self-contained attachment that would significantly improve the dynamic response of the NATA under typical operating conditions. "Lightweight" here must be construed as small with respect to the total translational mass m_t of the NATA. When the structure supporting the wing section was taken into account, it was found that $m_t = 12$ kg. To make the best use of available hardware, it was convenient to fix the mass of the NES at $m_s = 1.2$ kg, corresponding to a mass ratio, in heave, of $m_s/m_t = 10\%$. Because of the manner in which the wing is supported in the NATA, it was possible to regard the NES as interacting directly with only the heave degree of freedom of the wing; that is, the NES was effectively mounted at the elastic axis of the NATA wing. (The analysis of Part 1 [17] suggests that it would in general be better to attach the NES away from the wing's elastic axis, but to achieve that with the NATA would require much more extensive modifications.)

With the mass fixed, preliminary design of the NES was reduced to the specification of the linear viscous damping coefficient c_s and the essentially nonlinear spring stiffness k_s coupling the NES mass m_s to the NATA plunge displacement $h(t)$. The ranges of values of these two parameters that could be readily produced with the existing NES had been established in earlier experiments on other (non-aerodynamic) NES applications, and data were available relating nonlinear stiffness and coupling efficiency at low structural frequencies. On this basis, values of the stiffness and damping were selected, then refined through a series of numerical simulations carried out using MATLAB.

The coupled equations of motion of the NATA and the NES are

$$\begin{bmatrix} M & 0 \\ 0 & m_s \end{bmatrix} \begin{Bmatrix} \ddot{x} \\ \ddot{v} \end{Bmatrix} + \begin{bmatrix} C & 0 \\ 0 & 0 \end{bmatrix} \begin{Bmatrix} \dot{x} \\ \dot{v} \end{Bmatrix} + \begin{bmatrix} K & 0 \\ 0 & 0 \end{bmatrix} \begin{Bmatrix} x \\ v \end{Bmatrix} = \begin{Bmatrix} F_c \\ 0 \end{Bmatrix} + \begin{Bmatrix} F_a \\ 0 \end{Bmatrix} + \begin{Bmatrix} F_s \\ -f_s \end{Bmatrix} \tag{6}$$

where M, C, K, and $x(t)$ are the mass, damping, and stiffness matrices and the displacement vector of the 2-DOF NATA, defined above, $v(t)$ is the NES displacement, F_c and F_a are friction and aerodynamic forces as before, and

$$F_s = \{-f_s \;\; 0\}^T \tag{7}$$

represents the force f_s exerted on the NATA (in plunge) by the NES. The NES dynamics are governed by

$$m_s \ddot{v}(t) = -f_s(t) \tag{8}$$

where

$$f_s = c_s(\dot{v} - \dot{h}) + k_s|v - h|^{2.8}\mathrm{sgn}(v - h) \tag{9}$$

The exponent shown, 2.8, is typical of the values experimentally identified for the (theoretically purely cubic) coupling spring.

The results of these simulations indicated that good performance could be achieved over a range of damping values and with nonlinear coupling stiffnesses among the lower values previously realized. Although the viscous damping coefficient c_s does affect the rate and amount of energy pumping in the combined system, the simulations were relatively insensitive to this parameter and so a value of 0.40 Ns/m, typical of damping levels previously identified, was chosen. Additional simulations showed values of k_s in the range $[1.0, 2.0] \times 10^6$ N/m$^{2.8}$ to produce an effective NES, with larger values in this range to be preferred for practical reasons, such as smaller relative displacements during testing. The values for a preliminary NES design are collected in Table 2.

The NES used with the NATA in the experiments described here consisted of a small "car" made of aluminum angle stock. The car was supported on an air track (fed with shop air at 4 atm) to reduce sliding friction in the system, and was connected to the NATA through the viscous damper and the essentially nonlinear spring. The spring was created by securing a pair of thin wires perpendicular to the relative movement of the NATA and the NES (i.e., to the heave motion of the NATA) as shown in Fig. 6. The wires were mounted with no initial tension and hence their spring force had no linear component. This arrangement of wires ensured that when the NATA moved with respect to the NES, tension was created in the wires, ideally providing a cubic restoring force between the two subsystems. The entire NES assembly was attached to the NATA plunge carriage through a rod. Figures 7 and 8, respectively, show the NES resting on the air track and installed on the NATA in line with the plunge carriage.

Table 2 Nominal NES parameter values. Actual values were identified and adjusted during testing

Parameter	Symbol	Value	Units
NES mass	m_s	1.2	kg
Viscous damping coefficient	c_s	0.40	Ns/m
Spring stiffness	k_s	1.6×10^6	N/m$^{2.8}$

C. Data Acquisition and Processing

The pitch and plunge motions of the aeroelastic system were measured with optical angular encoders attached to the cams of the NATA, whereas NES response was detected using an accelerometer and integrated numerically to obtain velocity and displacement signals as needed. The force developed between the NES and NATA was sensed by a piezoelectric force transducer; this signal was used only during some of the system identification procedures. Freestream velocity inside the wind tunnel was determined using a Pitot probe and an electronic pressure transducer. All of these signals were sent to a data acquisition board for recording on a PC.

III. Results and Discussion

The first step in performing experiments with the NATA and the NES was to set the wind tunnel to the desired freestream velocity. Next, the initial conditions were imposed by manually displacing the NATA plunge carriage (and thus the NES) and waiting until equilibrium was established. The system was then released and the responses measured.

When the flow speed in the wind tunnel exceeded the NATA's flutter speed, approximately 9.5 m/s, an LCO could be reliably induced by releasing the wing from an initial heave displacement h_0, with all other initial conditions (pitch angle and pitch and heave rates) zero. Because of the Coulomb friction in the system, very small values of h_0 (up to a few millimeters) were insufficient to trigger the wing's limit cycle response, but for all larger h_0 the development of the LCO was very consistent. In all the experiments conducted with the NATA and NES, the dynamic behavior of the system was initiated by such a static heave displacement. As a consequence of the kinematics of the NATA, these initial conditions produced no aerodynamic moment on the wing, and when the NES was present its initial displacement was equal to that of the plunge carriage, h_0.

The various combinations of flow speed, initial plunge displacement, and NES characteristics tested are summarized in Table 3. The mass of the NES was determined with a laboratory balance, while the stiffness of the essentially nonlinear coupling spring and the associated viscous damping coefficient were identified using the restoring force surface method [30]. The damping force produced by the motion of the NES car on the air track was by comparison very small, and has been neglected throughout this work. The ratio of the NES mass, 1.2 or 1.5 kg, to the translational mass of the NATA was 10 or 12.5%, respectively. Although these may be unrealistically large values for flight hardware, they are not unreasonable for purposes of validating the analysis given in the companion paper, Part 1 [17]. The analysis

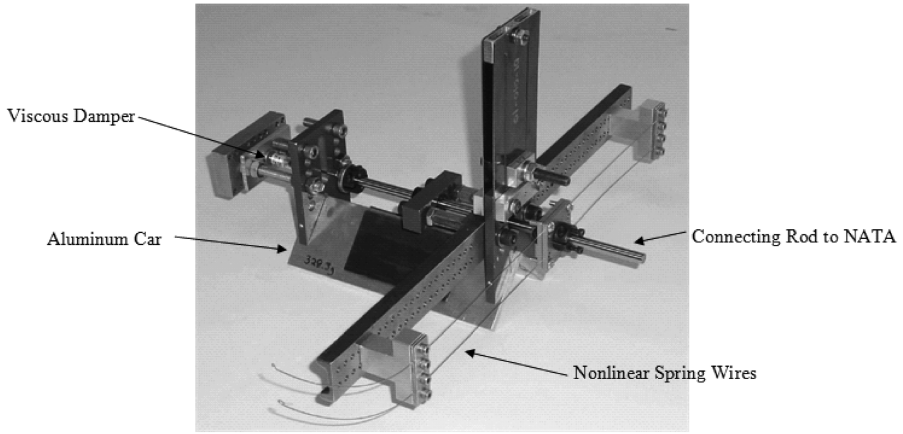

a)

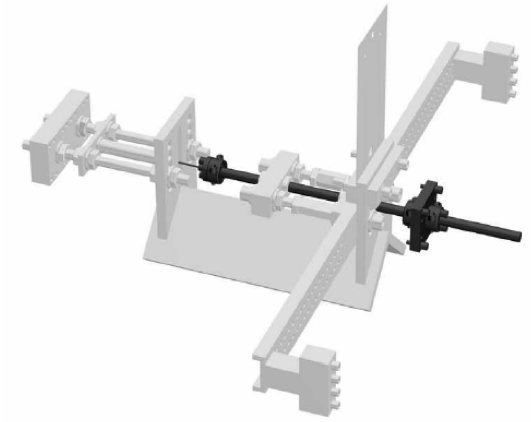

b)

Fig. 6 The nonlinear energy sink (NES): a) hardware used with the NATA; b) mass partition (the dark portion moved with wing plunge motion, while the light portion constituted the NES mass).

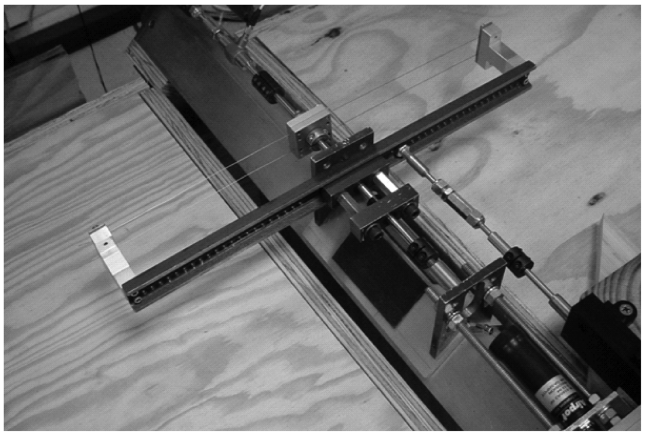

Fig. 7 The NES at rest on the air track. The connecting rod to the NATA is visible at the top. Wing heave and NES motion are parallel to the track.

discussed there treats an NES of finite mass, and it clearly indicates that energy transfer performance will not be degraded as the sink mass is made smaller.

A. Summary of Time-Response Data

Time histories of the heave and pitch responses of the various configurations at several flow speeds are shown in insets within Figs. 9–11. In each case, the response of the NATA with no NES is shown for reference. On these are superimposed responses with the NES attached, which demonstrate the three LCO suppression mechanisms discussed in Part 1 [17] of this study: 1) recurring burst out and suppression; 2) intermediate (partial) suppression; and 3) complete elimination. The steady-state amplitudes of the LCOs, if any, are plotted in these figures as discrete points for each flow speed at which tests were conducted (9, 10, 11, 12, and 13 m/s). When the amplitude of an LCO response exhibited modulation (i.e., the first suppression mechanism was observed), a pair of points has been plotted to indicate the range of the response envelope.

It is clear from these figures that, with no NES attached, the NATA was stable at a flow speed of 9 m/s. At this speed, the heave and pitch responses following an initial heave displacement of either 1.27 or 1.91 cm (with other initial conditions zero) decayed to the original static equilibrium. When the flow was increased to $U = 10$ m/s or more, the NATA's response to initial displacement of either magnitude exhibited a highly repeatable limit cycle, with amplitude and frequency depending on U. These findings are consistent with earlier estimates of $U_f = 9.5$ m/s for the flutter speed of the NATA. The precise flutter speed is of limited interest here; it was enough to show that robust LCO existed at $U = 10$ m/s and above before the NES was attached.

Concerning the LCO triggering mechanism [18] in the NATA, we observe that there was a nonlinear interaction between the two aeroelastic modes through a 1:1 internal resonance. Although the dynamics did not involve a stage of superharmonic resonance capture for the particular parameters (e.g., frequency ratio) of the NATA as configured for these tests, it did display a phase-locked frequency shift with time (and thus with increased energy fed into the system from the freestream).

The dashed lines in Fig. 9 connect points representing the LCO amplitudes observed for the NATA after connection of an NES with parameters having the baseline values show in boldface in Table 3.

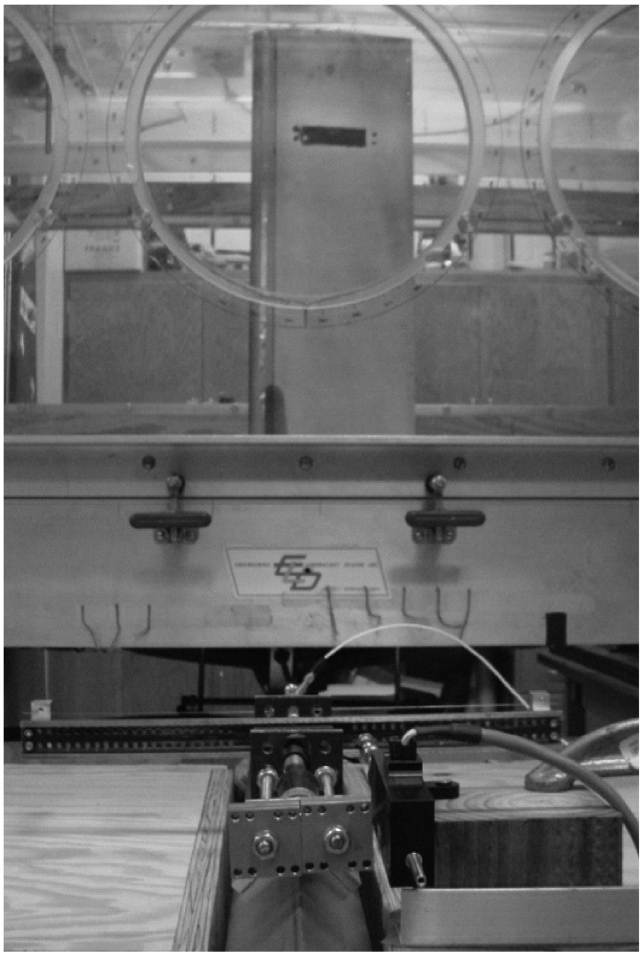

Fig. 8 The NES and air track structure mounted to the wind-tunnel frame of the NATA. Wing heave and NES motion are out of the page.

This configuration had the smaller mass ($m_s = 1.2$ kg), weaker essentially nonlinear coupling stiffness ($k_s = 1.6 \times 10^6$ N/m$^{2.8}$), and smaller damping coefficient ($c_s = 0.015$ Ns/m) of the values tested. From the figure, we immediately note a remarkable improvement in flutter speed, from 9 to 11 m/s, achieved for either initial heave displacement (1.27 or 1.91 cm). Accompanying the increase in flow speed beyond 11 m/s is a transition from complete LCO suppression to intermediate suppression (i.e., LCO with an amplitude less than that observed in the NATA with no NES). We also observe that while the response amplitude decays almost exponentially when $U = 10$ m/s, the decay is slower and the dynamics more complicated when $U = 11$ m/s (although complete suppression is still achieved).

The effects of varying the initial conditions or NES parameters on the response of the combined system are generally in agreement with theoretical predictions that increasing the NES mass and decreasing the damping or nonlinear stiffness tend to simplify the bifurcation behaviors of the steady-state dynamics and thus increase the robustness of LCO suppression. It is difficult to formulate simple rules describing these influences because of the high dimension of the phase space and the possible presence of subcritical LCO behavior, discussed in Part 1 [17]. However, we can make the following observations:

1) Stronger nonlinear coupling stiffness reduces the dependence of LCO suppression on the amplitude of the initial displacement.

2) Weaker nonlinear coupling stiffness can result in higher flutter speeds (i.e., in complete LCO suppression at higher flow speeds).

3) Greater NES damping usually produces better LCO suppression, although this may come at the expense of increased sensitivity to initial conditions.

4) Increasing the mass of the NES improved its performance following the smaller initial heave displacement, but the larger initial condition then produced more complex (and generally inferior) results. This is consistent with earlier findings that sinks of this configuration will actually benefit from having a small mass ratio, and suggests that the mass of the NES used in this study was rather large compared to the actual optimum value.

Of course, because of the complexity of the bifurcation structure introduced by the NES these points may not apply when the

Table 3 Experimental conditions and identified NES parameter values. Baseline values are in boldface

Parameter	Value
Freestream speed U	9–13 m/s
Initial heave displacement $h(0)$	1.27 cm (0.50 in.), 1.91 cm (0.75 in.)
NES mass m_s	**1.2**, 1.5 kg
Nonlinear stiffness k_s	**1.6×10^6**, 2.0×10^6 N/m$^{2.8}$
NES damping c_s	**0.015**, 0.040 Ns/m

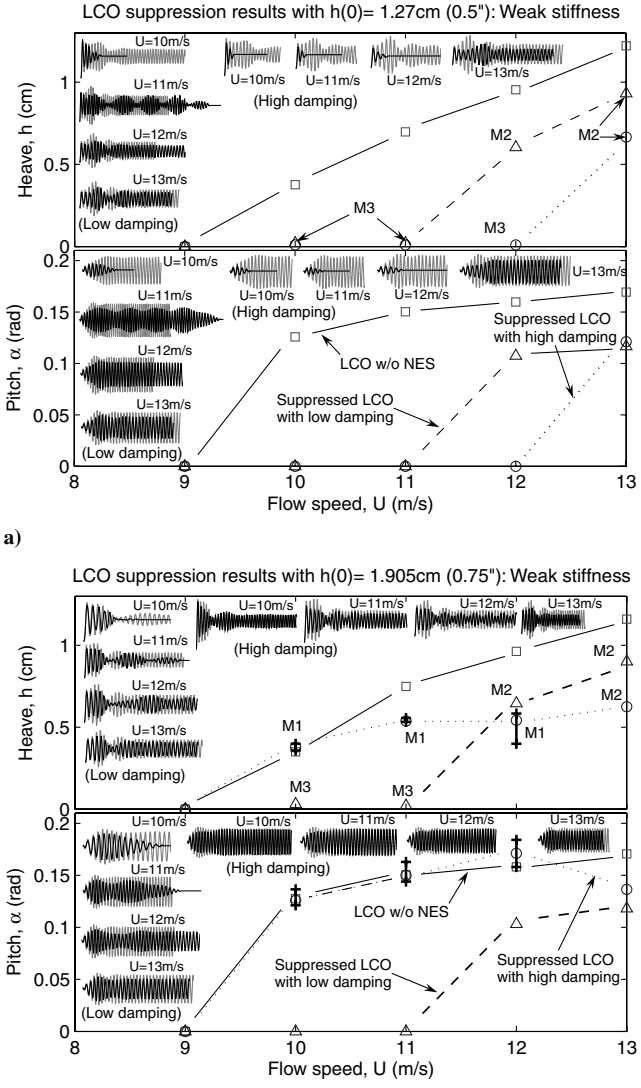

Fig. 9 Experimental responses (gray: without NES; black: with NES) obtained with the smaller NES mass ($m_s = 1.2$ kg) and weaker nonlinear stiffness ($k_s = 1.6 \times 10^6$ N/m$^{2.8}$): a) $h(0) = 1.27$ cm; b) $h(0) = 1.91$ cm. Steady-state amplitudes are indicated by □, NATA without NES; △, NATA and NES with lower damping ($c_s = 0.015$ Ns/m); ○, NATA and NES with higher damping ($c_s = 0.040$ Ns/m). Minimum and maximum values of modulated amplitude are indicated by pairs of + symbols. M1, M2, and M3 indicate the suppression mechanism at work.

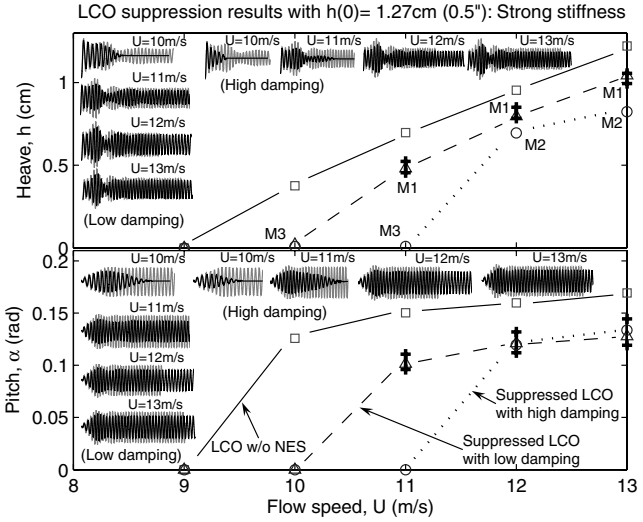

a)

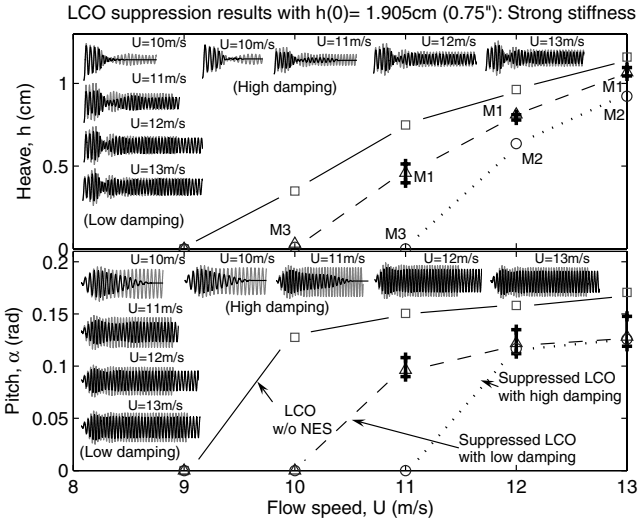

b)

Fig. 10 Experimental responses (gray: without NES; black: with NES) obtained with the smaller NES mass ($m_s = 1.2$ kg) and stronger nonlinear stiffness ($k_s = 2.0 \times 10^6$ N/m$^{2.8}$): a) $h(0) = 1.27$ cm; b) $h(0) = 1.91$ cm. Steady-state amplitudes are indicated by □, NATA without NES; △, NATA and NES with lower damping ($c_s = 0.015$ Ns/m); ○, NATA and NES with higher damping ($c_s = 0.040$ Ns/m). Minimum and maximum values of modulated amplitude are indicated by pairs of + symbols. M1, M2, and M3 indicate the suppression mechanism at work.

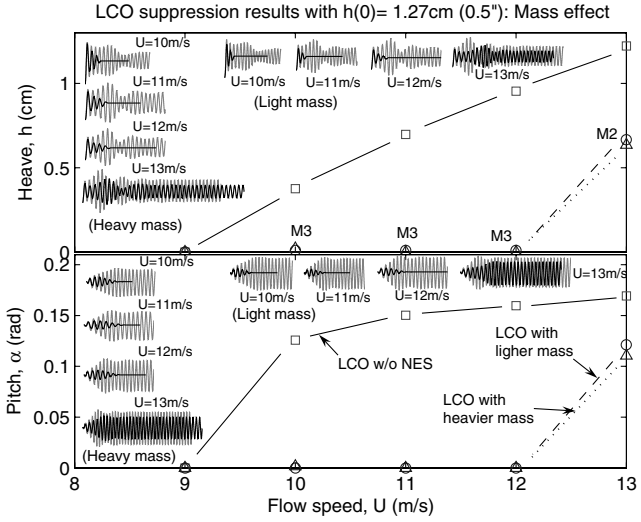

a)

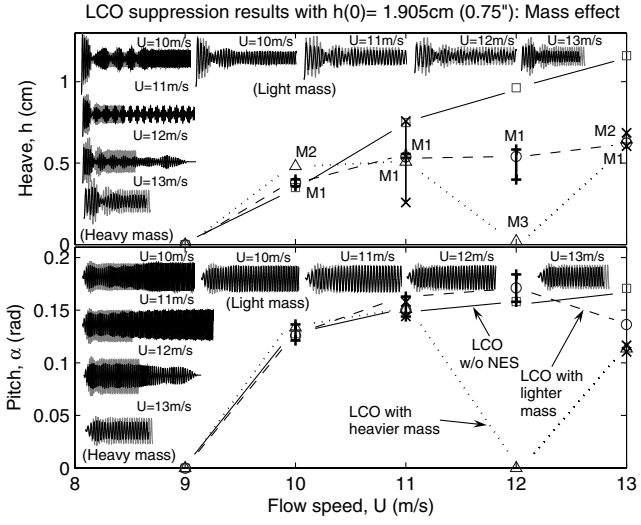

b)

Fig. 11 Experimental responses (gray: without NES; black: with NES) obtained with the larger NES mass ($m_s = 1.5$ kg) and weaker nonlinear stiffness ($k_s = 1.6 \times 10^6$ N/m$^{2.8}$): a) $h(0) = 1.27$ cm; b) $h(0) = 1.91$ cm. Steady-state amplitudes are indicated by □, NATA without NES; △, NATA and NES with lower damping ($c_s = 0.015$ Ns/m); ○, NATA and NES with higher damping ($c_s = 0.040$ Ns/m). Minimum and maximum values of modulated amplitude are indicated by pairs of + symbols. M1, M2. and M3 indicate the suppression mechanism at work.

operating conditions or NES parameter values are much different from those tested.

B. Identified LCO Suppression Mechanisms

Figure 12 depicts the first suppression mechanism, observed at $U = 11$ m/s with an NES of lighter mass, weaker nonlinear coupling stiffness, and higher damping. In agreement with theory, both the aeroelastic modes and the NES response exhibit nonlinear beating, that is, recurring burst out and suppression of instability occurs.

The frequencies of the aeroelastic modes exhibit a 1:1 relationship, initially around 2 Hz and later sustained at about 3 Hz. This can be most clearly seen in Fig. 12b, which depicts frequency vs time as computed by taking the wavelet transforms (WTs) of the time responses in Fig. 12a. The ratio between the NES frequency and that of the heave mode, and between the NES and the pitch mode, is 1:2. This suggests that this suppression mechanism consists primarily of recurring transient subharmonic resonance captures between the NES and the aeroelastic modes, while the two aeroelastic modes remain continually in 1:1 internal resonance.

Figure 13 shows the energy exchanges between these modes and the NES. The instantaneous energy was computed as the sum of the kinetic and potential energies and normalized by the total energy in the system. The underlying triggering mechanism is that of Lee et al. [18], where energy is fed into the heave mode from the flow and then produces the pitch response. The NES interacts transiently with the heave mode at the onset of this pitch response ($0 < t < 7$ s), preventing full development of the LCO. Almost half the total energy is transferred to the NES within 2 s. Subharmonic resonance capture is generally less efficient than 1:1 resonance capture for energy transfer, and we conjecture that in the responses considered here the 1:2 subharmonic resonance captures between the NES and the aeroelastic modes were not sufficient to inhibit the 1:1 internal resonance of those modes.

Figure 14 depicts the second suppression mechanism, intermediate suppression, observed when $U = 13$ m/s, with an NES of lighter mass, weaker nonlinear coupling stiffness, and higher

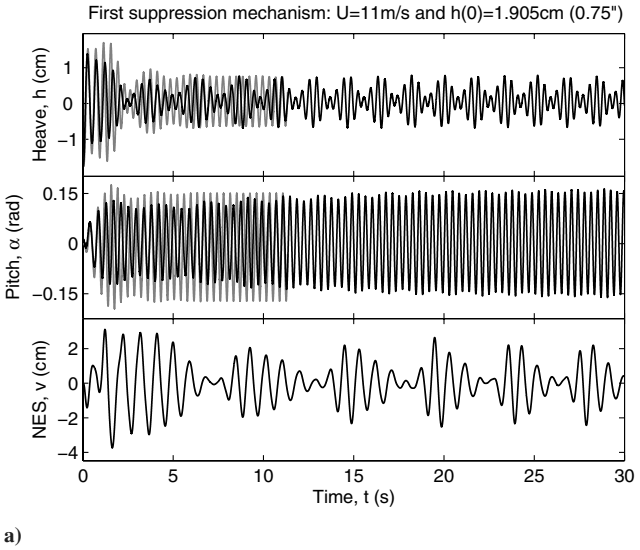

a)

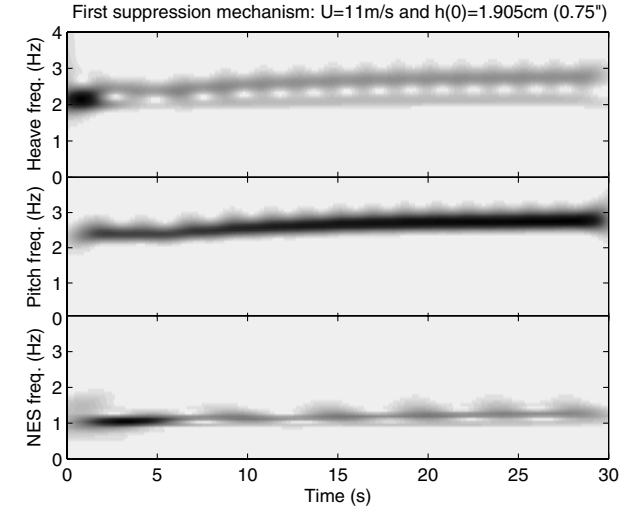

b)

Fig. 12 Typical responses showing the first LCO suppression mechanism: a) time histories; and b) wavelet transform magnitudes. $U = 11$ m/s; NES: heavy mass, weak coupling, and high damping; $h(0) = 1.91$ cm.

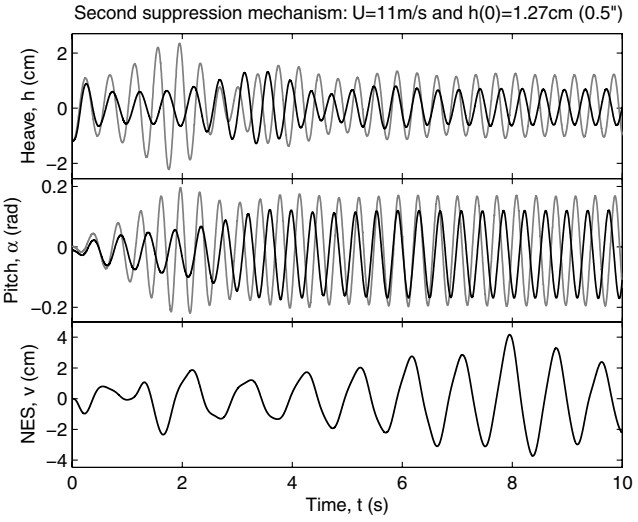

a)

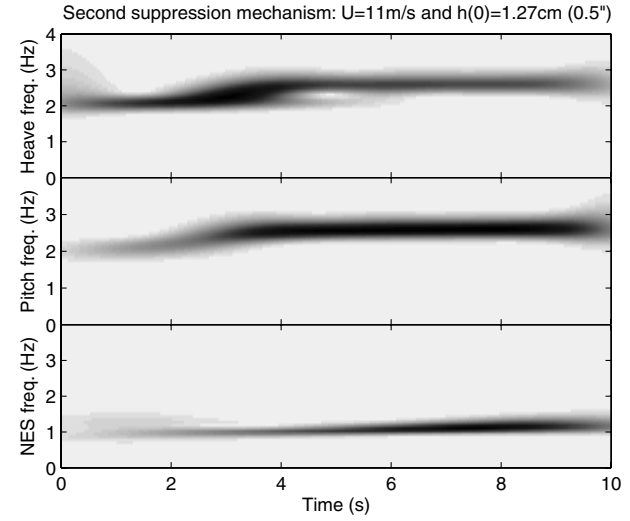

b)

Fig. 14 Typical responses showing the second LCO suppression mechanism: a) time histories; and b) wavelet transform magnitudes. $U = 13$ m/s; NES: light mass, weak coupling, and high damping; $h(0) = 1.27$ cm.

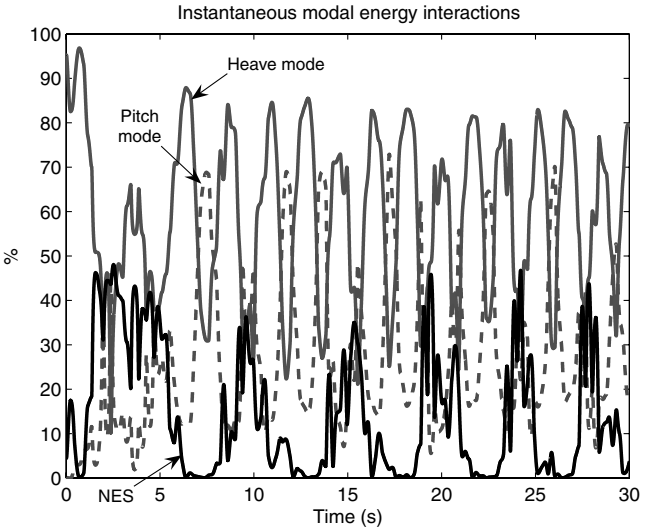

Fig. 13 Energy exchanges between modes in the first LCO suppression mechanism.

damping. After the initial transients die out, this system exhibits steady LCO of reduced amplitude (compared to the NATA without NES). Again, there exists strong nonlinear interaction between the heave and pitch modes through 1:1 internal resonance, and the NES undergoes 1:2 subharmonic resonance capture with the aeroelastic modes.

The third suppression mechanism, complete elimination of LCOs, is shown in Fig. 15 for a flow speed of $U = 10$ m/s, with a smaller NES mass, stronger nonlinear coupling, and higher damping. It is characterized by quick, complete elimination of aeroelastic instability. From the WT plot in Fig. 15b, it can be seen that while the aeroelastic modes are again in 1:1 internal resonance and the NES interacts with them in 1:2 subharmonic resonance as in the two cases discussed immediately above (suppression mechanisms 1 and 2), the NES also develops a 1:1 interaction with the heave mode. This 1:1 resonance capture suffices to eliminate the instability for this flow speed and initial disturbance.

Figure 16 shows another example of complete suppression. The flow speed has been increased to 11 m/s and the coupling stiffness reduced to its smaller value, with the result that LCO suppression is achieved only after several seconds of a modulated response which superficially resembles the bursting and suppression of the first mechanism. However, when the frequency content is examined, it is

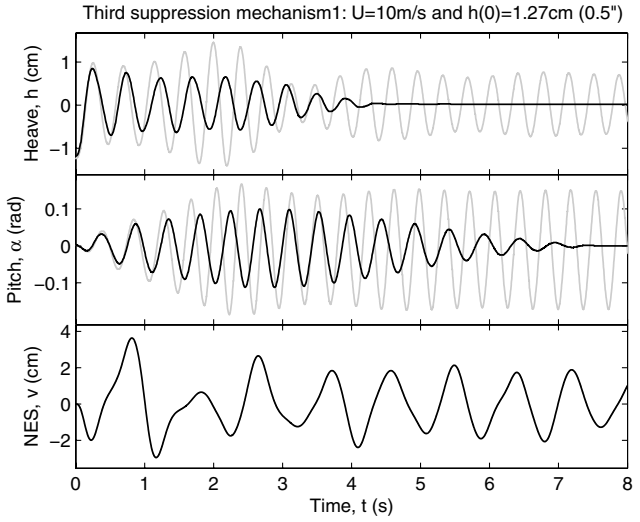

a)

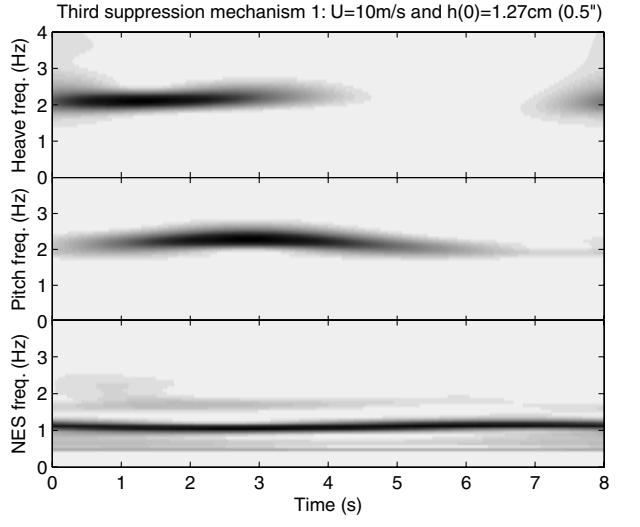

b)

Fig. 15 Typical responses showing the third LCO suppression mechanism: a) time histories; and b) wavelet transform magnitudes. $U = 10$ m/s; NES: light mass, strong coupling, and low damping; $h(0) = 1.27$ cm.

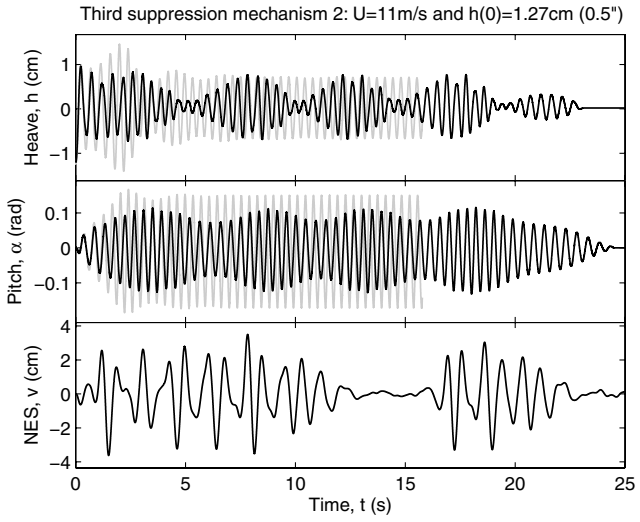

a)

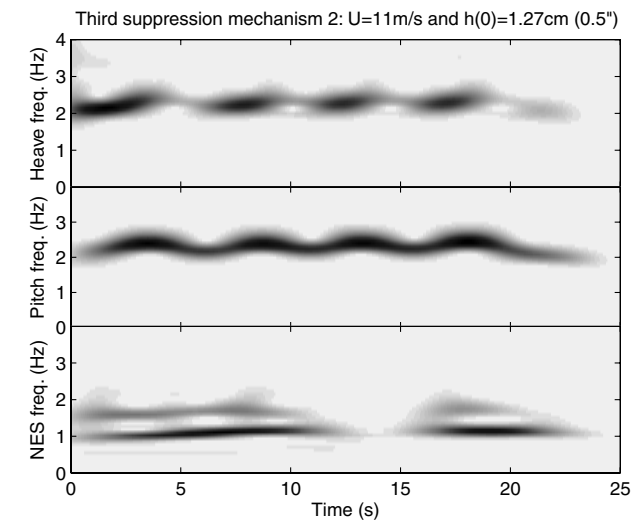

b)

Fig. 16 Third LCO suppression mechanism strongly affected by 1:1 internal resonance between the aeroelastic modes: a) time histories; and b) wavelet transform magnitudes. $U = 11$ m/s; NES: light mass, weak coupling, and low damping; $h(0) = 1.27$ cm.

found that the NES interacted with both aeroelastic modes, ultimately overcoming the 1:1 internal resonance between the heave and pitch modes to stabilize the system.

IV. Conclusions

The experiments reported herein successfully validate several aspects of the theory presented in the companion paper, Part 1 [17]. The triggering of aeroelastic instability in the NATA is due to 1:1 internal resonance between the heave and pitch modes; there is no transition to superharmonic resonance capture because the ratio of the natural frequencies of these modes is close to unity. With the NES attached at the elastic axis of the NATA, the main LCO branches of the NATA are preserved, and there still exist aeroelastic instabilities. However, the NES induces other branches through degenerate high-codimensional bifurcations, and these new branches are responsible for the three LCO suppression mechanisms. The key to achieving LCO suppression with the NES is to design a device that will interact strongly with the aeroelastic modes through 1:1 resonance captures. Increasing the mass of the NES and decreasing its damping and essentially nonlinear stiffness tend to simplify the bifurcation structure of the steady-state dynamics and thus to increase the robustness of LCO suppression. The data presented herein show that the NES improved the stability of the NATA wing, suppressing LCO at flow speeds up to 12 m/s, significantly faster than the wing's original critical speed of 9.5 m/s, without introducing undesirable new dynamics.

Acknowledgments

This work was funded in part by the U.S. Air Force Office of Scientific Research Contract Number FA9550-04-1-0073. G. Kerschen's participation was made possible by a grant from the Belgian National Fund for Scientific Research (FNRS). This support is gratefully acknowledged.

References

[1] Denegri, C. M., Jr., "Limit Cycle Oscillation Flight Test Results of a Fighter with External Stores," *Journal of Aircraft*, Vol. 37, No. 5, 2000, pp. 761–769.

[2] Bunton, R. W., and Denegri, C. M., Jr., "Limit Cycle Oscillation Characteristics of a Fighter Aircraft," *Journal of Aircraft*, Vol. 37, No. 5, 2000, pp. 916–918.

[3] Croft, J., "Airbus Elevator Flutter: Annoying or Dangerous?," *Aviation Week and Space Technology*, Vol. 155, No. 9, 2001, p. 41.

[4] Dowell, E. A., Edwards, J., and Strganac, T. W., "Nonlinear Aeroelasticity," *Journal of Aircraft*, Vol. 40, No. 5, 2003, pp. 857–874.

[5] Cunningham, A. M., Jr., "The Role of Non-Linear Aerodynamics in Fluid-Structure Interaction," AIAA Paper 98-2423, 1998.
[6] Hartwich, P. M., Dobbs, S. K., Arslan, A. E., and Kim, S. C., "Navier-Stokes Computations of Limit Cycle Oscillations for a B-1-Like Configuration," AIAA Paper 2000-2338, 2000.
[7] Chen, P. C., Sarhaddi, D., and Liu, D. D., "Limit Cycle Oscillation Studies of a Fighter with External Stores," AIAA Paper 98-1727, 1998.
[8] Gilliatt, H. C., Strganac, T. W., and Kurdila, A. J., "An Investigation of Internal Resonance in Aeroelastic Systems," *Nonlinear Dynamics*, Vol. 31, No. 1, Jan. 2003, pp. 1–22.
[9] Thompson, D. E., Jr., and Strganac, T. W., "Store-Induced Limit Cycle Oscillations and Internal Resonances in Aeroelastic Systems," AIAA Paper 2000-1413, 2000.
[10] Tang, D., and Dowell, E., "Experimental and Theoretical Study on Aeroelastic Response of High-Aspect-Ratio Wings," *AIAA Journal*, Vol. 39, No. 8, 2001, pp. 1430–1441.
[11] O'Neil, T., "Nonlinear Aeroelastic Response—Analyses and Experiments," AIAA Paper 96-0014, 1996.
[12] O'Neil, T., Gilliatt, H., and Strganac, T. W., "Investigations of Aeroelastic Response for a System with Continuous Structural Nonlinearities," AIAA Paper 96-1390, 1996.
[13] Sheta, E. F., Harrand, V. J., Thompson, D. E., and Strganac, T. W., "Computational and Experimental Investigation of Limit Cycle Oscillations in Nonlinear Aeroelastic Systems," AIAA Paper 2000-1399, 2000.
[14] Ko, J., Strganac, T. W., and Kurdila, A. J., "Adaptive Linearization for the Control of a Typical Wing Section with Torsional Nonlinearity," *Nonlinear Dynamics*, Vol. 18, No. 3, March 1999, pp. 289–301.
[15] Block, J. J., and Strganac, T. W., "Applied Active Control for a Nonlinear Aeroelastic Structure," *Journal of Guidance, Control, and Dynamics*, Vol. 21, No. 6, 1998, pp. 838–845.
[16] Platanitis, G., and Strganac, T. W., "Control of a Nonlinear Wing Section Using Leading- and Trailing-Edge Surfaces," *Journal of Guidance, Control, and Dynamics*, Vol. 27, No. 1, 2004, pp. 52–58.
[17] Lee, Y. S., Vakakis, A. F., Bergman, L. A., McFarland, D. M., and Kerschen, G., "Suppressing Aeroelastic Instability Using Broadband Passive Targeted Energy Transfers, Part 1: Theory, *AIAA Journal*, Vol. 45, No. 3, March 2007, pp. 693–711.
[18] Lee, Y. S., Vakakis, A. F., Bergman, L. A., McFarland, D. M., and Kerschen, G., "Triggering Mechanisms of Limit Cycle Oscillations due to Aeroelastic Instability," *Journal of Fluids and Structures*, Vol. 118, No. 2, Aug. 2005, pp. 791–799.
[19] Gendelman, O., "Transition of Energy to a Nonlinear Localized Mode in a Highly Asymmetric System of Two Oscillators," *Nonlinear Dynamics*, Vol. 25, Nos. 1–3, 2001, pp. 237–253.
[20] Gendelman, O., Manevitch, L. I., Vakakis, A. F., and M'Closkey, R., "Energy Pumping in Nonlinear Mechanical Oscillators: Part 1—Dynamics of the Underlying Hamiltonian Systems," *Journal of Applied Mechanics*, Vol. 68, Jan. 2001, pp. 34–41.
[21] Vakakis, A. F., and Gendelman, O., "Energy Pumping in Nonlinear Mechanical Oscillators: Part 2—Resonance Capture," *Journal of Applied Mechanics*, Vol. 68, Jan. 2001, pp. 42–48.
[22] Vakakis, A. F., Manevitch, L. I., Gendelman, O., and Bergman, L. A., "Dynamics of Linear Discrete Systems Connected to Local, Essentially Nonlinear Attachments," *Journal of Sound and Vibration*, Vol. 264, No. 3, July 2003, pp. 559–577.
[23] Vakakis, A. F., McFarland, D. M., Bergman, L. A., Manevitch, L. I., and Gendelman, O., "Isolated Resonance Captures and Resonance Capture Cascades Leading to Single- or Multi-Mode Passive Energy Pumping in Damped Coupled Oscillators," *Journal of Vibration and Acoustics*, Vol. 126, No. 2, April 2004, pp. 235–244.
[24] Kerschen, G., Kowtko, J. J., McFarland, D. M., Bergman, L. A., and Vakakis, A. F., "Theoretical and Experimental Study of Multimodal Targeted Energy Transfer in a System of Coupled Oscillators," *Nonlinear Dynamics*, Vol. 47, Nos. 1–3, 2007, pp. 285–309.
[25] Kerschen, G., Lee, Y. S., Vakakis, A. F., McFarland, D. M., and Bergman, L. A., "Irreversible Passive Energy Transfer in Coupled Oscillators with Essential Nonlinearity," *SIAM Journal on Applied Mathematics*, Vol. 66, No. 2, 2006, pp. 648–679.
[26] Kerschen, G., McFarland, D. M., Kowtko, J. J., Lee, Y. S., Bergman, L. A., and Vakakis, A. F., "Experimental Demonstration of Transient Resonance Capture in a System of Two Coupled Oscillators with Essential Stiffness Nonlinearity," *Journal of Sound and Vibration*, Vol. 299, Nos. 4–5, 2007, pp. 822–838.
[27] McFarland, D. M., Bergman, L. A., and Vakakis, A. F., "Experimental Study of Nonlinear Energy Pumping Occurring at a Single Fast Frequency," *International Journal of Nonlinear Mechanics*, Vol. 40, No. 6, July 2005, pp. 891–899.
[28] McFarland, D. M., Kerschen, G., Kowtko, J. J., Bergman, L. A., and Vakakis, A. F., "Experimental Investigation of Targeted Energy Transfers in Strongly and Nonlinearly Coupled Oscillators," *Journal of the Acoustical Society of America*, Vol. 118, No. 2, Aug. 2005, pp. 791–799.
[29] Lee, Y. S., Vakakis, A. F., Bergman, L. A., and McFarland, D. M., "Suppression of Limit Cycle Oscillations in the van der Pol Oscillator by Means of Passive Nonlinear Energy Sinks (NESs)," *Structural Control and Health Monitoring*, Vol. 13, No. 1, 2006, pp. 41–75.
[30] Masri, S. F., and Caughey, T. K., "Nonparametric Identification Technique for Nonlinear Dynamic Systems," *Journal of Applied Mechanics*, Vol. 46, June 1979, pp. 433–447.

M. Ahmadian
Associate Editor